Exciton lasing in carbon nanotubes below the population-inversion threshold via phonon-mediated stimulated emission

Stefano Dal Forno [*] and Marco Battiato[†]

School of Physical and Mathematical Sciences, Nanyang Technological University, 50 Nanyang Ave, Singapore 639798

Excitonic optical transitions in carbon nanotubes (CNTs) have been extensively studied for at least two decades. However, exploiting these transitions to produce a lasing effect has proven to be unpractical due to the difficulties of achieving an excitonic population inversion in carbon nanotubes. In this work we show that lasing is theoretically possible at a much lower exciton population threshold by taking advantage of phonon stimulated emission. Specifically, the so-called anti-Stokes transitions, where light is generated by the creation of a phonon and the annihilation of an exciton, can be used to sustain the coherent emission of photons. These transitions have been overlooked for long due to their low intensity as a consequence of the low occupancy of the associated phonon branches. We show that the best conditions to achieve the lasing effect are met in CNTs with (i) excitons of nonzero momentum, (ii) a strong exciton-phonon coupling, and (iii) narrow exciton transitions.

I. INTRODUCTION

Single-wall carbon nanotubes (SWCNTs) are viable systems for a range of electronic and optical applications due to their size and distinctive mechanical, chemical, and electronic properties. The lowest-lying photoexcitations in semiconducting SWCNTs are strongly bound, one-dimensional excitons with binding energies up to 0.5 eV depending on chirality and diameter [1]. SWCNTs have attracted a lot of attention because of the distinctive optical properties that result from their nearly ideal one-dimensional geometry. The mechanisms of light emission in SWCNTs have been widely explored and include light-emitting diodes [2], photoluminescence spectroscopy [3], THz emitters and detectors [4,5], single-photon sources [6], defect doping [7], exciton trapping [8], population inversion of hot electrons [9], Auger processes [10,11], and Raman scattering [12].

However, an excitonic-population-inversion effect capable of efficiently sustaining coherent light emission in SWCNTs has not yet been achieved. For example, Lüer *et al.* [13] demonstrated that with a laser fluence of 4 μJ/cm^2 (corresponding to an exciton density of 2×10^{13} excitons/cm^2), only 12% of the total exciton population phase space is occupied. At this rate, the complete phase space filling would occur at 2×10^{14} excitons/cm^2, but this in fact does not happen because of saturation effects limiting the population-inversion process. This saturation effect is a consequence of scattering processes involving defects, phonons, and most importantly, nonradiative dark excitons. Because of this, the exciton population decays in a strongly dispersive manner with exciton lifetimes that are less than 10 ps [14]. This feature undermines the attempts to achieve an excitonic population inversion.

However, a comparison with other low-dimensional systems suggests that a lasing effect can be achieved with the help of anti-Stokes Raman scattering [15–20]. In a *forward* anti-Stokes process light is absorbed, an exciton is created, and a phonon is annihilated. These transitions have always been overlooked due to their low intensity. This is a consequence of the fact that, at room temperature, the population of high-energy phonons is extremely low and this prevents measurements of anti-Stokes transitions in individual nanotubes [21]. On the other hand, a *reverse* anti-Stokes process is also possible: the emission of light by the creation of a phonon and the annihilation of an exciton. This mechanism is at the core of research developments in resonant CNT optical microcavities [22].

In this work we model the absorption and emission of light in CNTs by solving the full quantum Boltzmann equation. We employ our method to the example case of (6,5) SWCNTs but our conclusions remain general. We show that coherent light emission in CNT samples is possible. We show that this effect can be achieved at a much lower exciton density without the requirement of a complete exciton phase space filling. This mechanism is driven by the emission of anti-Stokes phonons. We explore a wide range of initial configurations and determine the optimal conditions under which coherent light emission is achieved. Our model predicts that light emission is more efficient at (i) low temperatures, (ii) in the presence of many excitons with nonzero momentum, (iii) in cases of strong exciton-phonon coupling, and (iv) when the main exciton peak is narrower than the phonon sidebands. Our findings are supported by an excellent agreement with pump-probe experiments for low exciton densities. Most importantly, our model does not use any close-to-equilibrium approximation to describe the exciton and phonon populations [23–25].

II. METHODS

A lasing effect is achieved when the process of stimulated emission overcomes the spontaneous emission and absorption of a particular transition. In practice, determining under which

---

*Contact author: tenobaldi@gmail.com
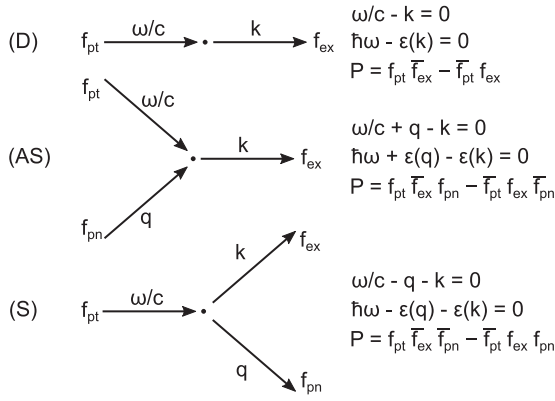†Contact author: marco.battiato@ntu.edu.sg

FIG. 1. Scattering mechanisms in this work.

FIG. 2. Absorption spectrum at equilibrium.

condition we could obtain a net coherent light emission is equivalent to searching for regions of negative absorbance coefficient. In this work we model the absorbance of (6,5) SWCNTs in the frequency range around the E_{11} bright excitonic peak.

A. Involved optical transitions

The time evolution of the population of a system of (quasi)particles can be described by solving the full quantum Boltzmann equation. In the absence of external fields and by neglecting the spatial degrees of freedom this reads

$$\frac{\partial f_n}{\partial t} = \sum_\alpha \left(\frac{\partial f_n}{\partial t} \right)_\alpha, \tag{1}$$

where f_n represents the population of a particle labeled by the index n, and α runs over all the possible collision terms between such particles.

In a similar fashion to our previous work [25], we consider three families of collision terms:

(i) the direct absorption (D) of a photon into an exciton;

(ii) creation of an exciton via the absorption of a photon and a phonon (anti-Stokes process, AS);

(iii) and the creation of an exciton via the absorption of a photon and the emission of a phonon (Stokes process, S).

Figure 1 shows a pictorial description of the above scattering families and the parameters used in this model are listed in the Appendix for the reader's convenience.

We refer to f_{pt}, f_{ex}, and f_{pn} as the populations of photons, excitons, and phonons, respectively. Also, since we will describe the behavior of the system out of equilibrium, the populations will not be, in general, a Fermi-Dirac or a Bose-Einstein distribution.

Each transition is constrained by the fermionic or bosonic nature of the quasiparticles and its probability weighted by the population phase space factor P (see Fig. 1). We used the shortened notation $\overline{f_i} = 1 \pm f_i$, where the plus (minus) sign applies for a boson (fermion) quasiparticle. In this respect, it is important to mention that excitons behave as bosons at very low occupancy, but progressively become more fermionic at high populations [26]. However, in this work we are doing the simplifying assumption that excitons behave like fermions even for low occupancies. This approximation holds when Pauli blocking mechanisms start to become important
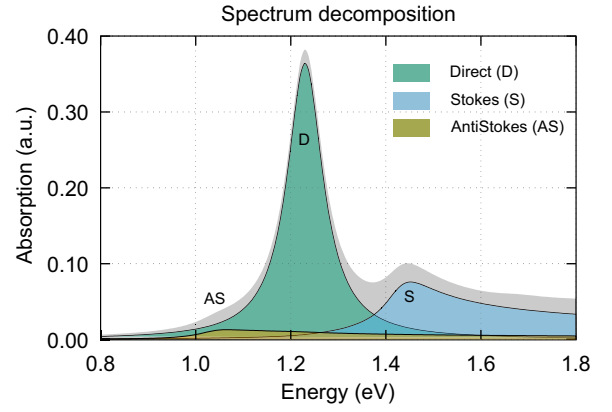
and, as already mentioned above, this happens at a relatively small filling factor [13] (see Supplemental Material for more details [27]).

Finally, the probability of a specific transition is proportional to the scattering matrix element (see Appendix for more details). However the most impactful factors influencing the spectral shape are the energy and momentum conservation relations, which are again summarized Fig. 1, where $\hbar\omega/c$, $\hbar k$, and $\hbar q$ are the momenta carried by the photon, exciton, and phonon, respectively, while $\hbar\omega$, $\epsilon(k)$, and $\epsilon_\nu(q)$ are their energy dispersion relations.

B. Absorption spectrum

The frequency-dependent absorbance $A(\omega)$ is

$$A(\omega) \propto \sum_\alpha \lambda_\alpha(\omega) = \lambda_D(\omega) + \lambda_{AS}(\omega) + \lambda_S(\omega). \tag{2}$$

In the above equation, $\lambda_\alpha(\omega)$ represents the scattering rate of the photon population, i.e., the *probability rate* of a photon to be absorbed (or emitted) as a consequence of the interaction with the excitons and phonons. The label $\alpha = \{D, AS, S\}$ represents one of the three possible scattering events we consider in our model.

The scattering rates $\lambda_\alpha(\omega)$ are calculated in terms of Boltzmann integrals. A full derivation of these integrals is given in Refs. [24,25] and it is summarized in the Appendix for the reader's convenience. As an example, we can write the scattering rate of a Stokes process as

$$\lambda_S(\omega) = \frac{2\pi}{\hbar} \frac{1}{V_{BZ}} \sum_{\mathbf{G}} \int_{V_{BZ}^2} d\mathbf{k}\,d\mathbf{q}\, |g_S|^2 \, \delta_{\mathbf{k}} \, \delta_\epsilon \, P', \tag{3}$$

where V_{BZ} is the volume of the Brillouin zone, $|g_S|^2$ is the matrix element of the transition, $\delta_{\mathbf{k}}$ and δ_ϵ enforce momentum and energy conservation, the summation over $\mathbf{G}$ takes umklapp scattering into account, and $P' = \delta P/\delta f_{pt}$ is the derivative of the population factors in Fig. 1.

Figure 2 shows the equilibrium absorption spectrum for (6,5) CNTs decomposed into the D, AS, and S components.

C. Approximated lasing thresholds

It is instructive to write down the integrated peak intensities for the considered processes,

$$\mathcal{I}_\alpha = \hbar \int \lambda_\alpha(\omega) d\omega. \tag{4}$$

This quantity is proportional to the total power absorbed by the α process; it can be directly measured in pump-probe experiments and can be used to estimate the density of excitons per unit length as a function of the laser fluence and the number of occupied exciton states [13]. Within this section we will assume nearly constant matrix elements and $\hbar V_{BZ} \ll 2m^*c$ (where m^* is the exciton effective mass). Under these approximations, the integrated peak intensity of the mentioned transitions can be evaluated.

In the case of direct absorption we can write

$$\mathcal{I}_D \sim \frac{2\pi}{\hbar} |g_D|^2 [1 - 2f_{ex}(\Gamma)], \tag{5}$$

where $f_{ex}(\Gamma)$ is the exciton population at the Γ point, $k = 0$. The absorption becomes negative when $f_{ex}(\Gamma) \geqslant 0.5$. This condition ensures the presence of lasing when the CNTs are placed in cavity resonant with the associated optical transition and corresponds to the usual requirement of population inversion for any conventional laser. As we have mentioned earlier, it has been shown experimentally that experimentally achievable exciton populations at the bottom of the E_{11} band are far smaller than this threshold, meaning that experimental approaches are still far from reaching excitonic populations that might sustain lasing.

If instead we look at the two phonon-assisted transitions, under the simplifying assumptions mentioned above, we obtain

$$\mathcal{I}_{AS} \sim \frac{2\pi}{\hbar} \frac{|g_{AS}|^2}{V_{BZ}} (N_{pn} - N_{ex} - 2N_{ex}N_{pn}), \tag{6}$$

$$\mathcal{I}_S \sim \frac{2\pi}{\hbar} \frac{|g_S|^2}{V_{BZ}} (1 + N_{pn} - N_{ex} - 2N_{ex}N_{pn}), \tag{7}$$

where $N_i = \int d\mathbf{k} f_i(\mathbf{k})$ is the total population of the ith species. For optical phonons at equilibrium and a sufficiently flat dispersion, N_{pn} is proportional to the Bose-Einstein distribution. Again, we must search for the condition where the integrated peak intensities are negative. We observe that for S transitions, Eq. (7) predicts a very large exciton population to achieve a negative absorption. On the other hand, Eq. (6) predicts that, in the case of low temperatures ($N_{pn} \sim 0$), any nonzero exciton population will produce a negative absorption for AS transitions. At sufficiently low temperatures, the threshold will be far lower than the requirement of population inversion for direct transitions.

While the above result is not completely preserved for more realistic situations, our accurate numerical study will lead to very similar conclusions even when the system is more realistically described.

D. Numerical details

We compute the above integrals using the TORTOISE package [23,24]. This tool is capable of solving the full

Boltzmann Equation without any close-to-equilibrium approximations. The numerical parameters used to describe the system are identical to the ones used in our previous published paper and are listed in the Appendix for the reader's convenience [25]. However, differently from the previous work, in this paper we explore a wide range of initial boundary conditions, with a particular focus on laser realization.

III. RESULTS AND DISCUSSION

To address the realistic thresholds for lasing in CNTs at different frequencies, we compute the absorption spectra as a function of some representative out-of-equilibrium excitonic populations. We chose the following test cases:
  (i) excitons generated optically by a laser,
  (ii) excitons in thermal equilibrium at a given temperature,
  (iii) excitons generated in doped CNTs,
  (iv) excitons in a highly nonthermal configuration.
As we will see later in this section, we have observed that only the value of the exciton population at Γ and the total number of excitons N_{ex} will play a primary role in our conclusions, while the other details will more marginally affect our results. For this reason, we choose to show only the absorbance obtained from excitons generated in doped CNTs, and show the remaining ones in the Supplemental Material [27].

Figure 3 shows the total absorbance obtained in a system of doped CNTs. The inset shows the actual form of the excitonic population and the corresponding chemical potential. Both panels (a) and (b) share some similar features: a main prominent peak at 1.24 eV (E_{11} exciton), and two phonon sidebands at ± 0.2 eV on the left and right of the main peak.

In panel (a) the exciton population has been kept fixed at thermal equilibrium at 300 K while the phonon population varies as a function of the temperature. We see that both the Stokes and anti-Stokes peaks increase as the phonon temperature increases (cf. dashed arrows). This behavior is confirmed by looking at Eq. (6) and Eq. (7), where the population factors of all transitions depend linearly on N_{pn} at the first leading order. Also, it is important to note the main exciton peak is unaffected by the phonon temperature.

The situation is much different for panel (b). In this case the phonon population has been kept fixed at thermal equilibrium at 300 K, while the exciton population varies with respect to the doping level (see inset). Specifically, we tuned the doping level by changing the exciton chemical potential from 0.99 eV (undoped) to 1.12 eV (very doped). We see that as the exciton population increases, the whole absorption spectrum greatly reduces. Specifically, we observe two important effects. The weakening of the main excitonic peak at 1.24 eV, also known as ground state (GS) bleaching, and a region of *negative absorbance* close to the anti-Stokes peak at ~ 1.05 eV, which represents the emission of light by the system. The first effect, also observed in the work by Lüer *et al.* [13], is caused by a Pauli blocking mechanism that forbids the creation of excitons at the Γ point and thus greatly reduces the absorption of light. As previously stated, this effect is maximum (i.e., zero absorbance) when the excitonic filling factor at the Γ point is 1/2. However, as already mentioned, such very high threshold for lasing is currently not experimentally achievable.
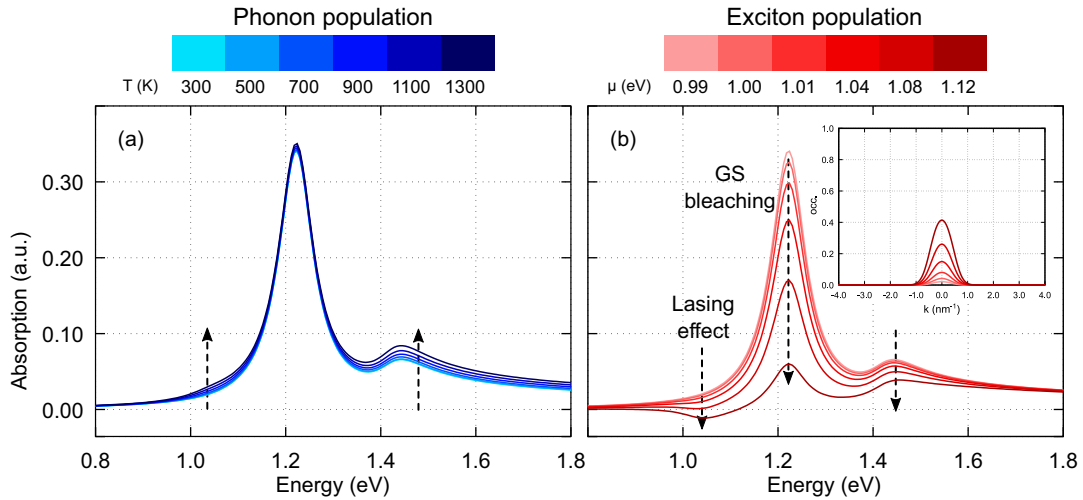
FIG. 3. Total spectra as a function of photon energy, phonon, and exciton populations.

The second and most important effect is the emission of light as a consequence of the exciton-phonon interaction. This effect causes excitons to decay by the emission of a photon and a phonon; see Fig. 1 (AS). We observe that, as stated earlier in the method section, the lasing threshold of this process is much lower than in the case of the GS bleaching. We start to observe a negative absorbance at a Γ filling factor of roughly 0.26 and a total exciton density of 0.24 nm^{-1} (cf. curve with 1.08 eV doping). These densities are lower than the theoretical population-inversion threshold, but still very high to achieve experimentally [13]. This is due to the overlap between the main and the AS peaks. As mentioned previously, the AS peak can become negative for any nonzero exciton population N_{ex}. However, the lasing effect is suppressed by the large positive absorption due to the tail of the main exciton peak. By looking at Fig. 2 and bearing in mind the lasing conditions from Eqs. (5) and (6), we see that we need a very high total exciton population N_{ex} so that the AS peak can overcome the absorption of the main peak. This suggests that, despite the predictions of Eq. (6), to achieve a lasing effect from the AS transition we need a narrow main exciton peak (i.e., long-lived excitons), a moderate filling factor at the Γ point, and many excitons with nonzero momentum (i.e., $N_{ex} > 0$).

Now we turn our attention to the integrated peak intensities of the individual transitions. Figure 4 shows the direct, anti-Stokes, and Stokes peak area as a function of the four test cases. Panel (a) shows that the D peak decreases linearly with a constant negative slope [cf. Eq. (5)]. Several very important findings can be extracted: (i) because of the form of Eq. (5), the slope is proportional to the value of the matrix element $|g_D|^2$ at the Γ point, (ii) the point of intersection at $x = 0$ equals $\hbar|g_D|^2/2\pi$, and (iii) the point of population inversion happens at exactly half occupancy $f_{ex}(\Gamma) = 1/2$. These findings are extremely important because they can be used to better interpret pump-probe experimental results. Specifically, one can estimate the coupling strength $|g_D|^2$ and calculate the number of excited excitons at Γ by a linear regression fit. Note however that these findings have to be considered with care, since we are neglecting second-order effects like two-photon excitations and single-particle electron-hole excitations.

Similarly, Figs. 4(b) and 4(c) show the individual dependence of the Stokes and anti-Stokes integrated intensities as functions of the phonon temperature (blue color scale) and exciton total population (x scale). The pink shaded region represent the region of negative absorbance, which becomes
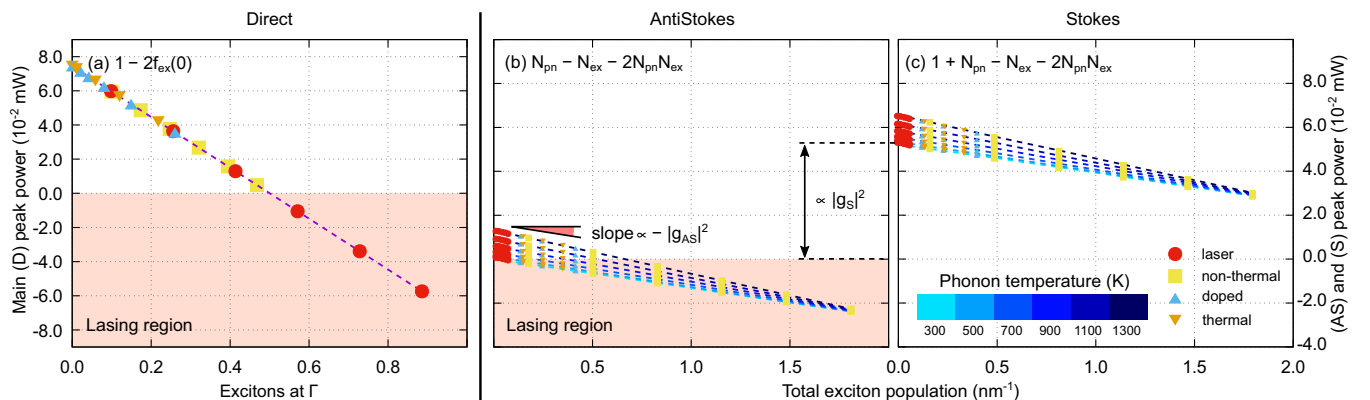

FIG. 4. D, AS, and S peak intensities versus phonon temperature and exciton population.
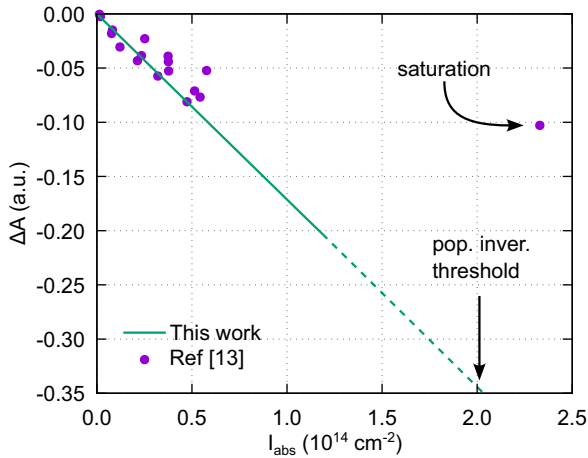
FIG. 5. Absorbance difference versus pump intensity.

TABLE I. Phonon modes and energies in meV.

nth mode	A	E_1	E_2
3rd	36.5 (RBM)	50.5	76.4
4th	110 (oTO)	109	108
5th	195 (G−)	194	189
6th	197 (G+)	195	192

available only to the AS transition. We observe two trends: (i) the integrated peak intensities decrease as a function of the exciton population, and (ii) the integrated peak intensities increase as function of the phonon population. Also, we see that the slope of the AS curve is proportional to the anti-Stokes coupling strength while the Stokes coupling strength is proportional to the power difference between the AS and S integrated peaks. These properties tell us that for an efficient lasing effect we need a strong exciton-phonon coupling and an efficient cooling of the sample.

Very interestingly, we also find that this effects depend on the total exciton population N_{ex} and does not depend on the actual form of the population function shown in the inset of Fig. 3 (see also the Supplemental Material [27]). This means that a broader excitonic population spanning many k states in the Brillouin zone will produce a stronger lasing effect. In practice, excitons with nonzero momentum (such as those arising from thermalization and secondary scattering events) are more likely to decay with the emission of an anti-Stokes phonon and a photon.

Finally, to validate our model, we compare our results to the pump-probe experimental data published by Lüer *et al.* [13] (see Supplemental Material [27] for details, and also Refs. [7,13,28]). Figure 5 shows an excellent agreement between our theory and the experimental data. We observe that for small exciton densities our model correctly reproduce the linear dependence between the exciton population and the D peak intensity. However, at high exciton densities our theory fails to describe the saturation effect visible at the far right side of Fig. 5 (cf. isolated point). There are a couple of reasons for this. First, the differential absorbance ΔA is a different quantity than the integrated peak intensity $\mathcal{I}_D$. Although they retain the same behavior for small laser fluences, they can diverge quite substantially depending on the broadening of the main peak and as a consequence of the overlap with the phonon sidebands. Second, the two quantities I_{abs} and $f_{ex}(\Gamma)$ are linearly dependent only for the ideal case of a Dirac-delta excitonic population centered at Γ. In real systems, thermalization effects, high laser fluences, and exciton-exciton and exciton-phonon scattering broaden the excitonic population.

IV. CONCLUSION

We investigated the optical properties of (6,5) SWCNTs and found that a lasing effect can be achieved via the decay of an exciton and the emission of a phonon. This process requires a much lower lasing activation threshold compared with the main direct excitonic transitions. However, in the specific case of (6,5) SWCNTs, this threshold is still not low enough to achieve experimentally. The main factors undermining the lasing effect are the vicinity and the broadening of the main excitonic peak. Thus, for an efficient lasing effect several conditions must be met: (i) a narrow main excitonic peak (i.e., long-lived excitons), (ii) a strong exciton-phonon coupling (higher power absorbed by the AS transition), (iii) an efficient cooling of the sample, and (iv) a high population of excitons with nonzero momentum. The latter can be achieved as a consequence of thermalization processes or scattering events. The power emitted is linearly proportional to the total exciton population.

APPENDIX: PARAMETERS OF THE MODEL

We describe the absorption (and emission) of light in (6,5) SWCNTs as a system of interacting excitons, phonons, and photons.

Band structure and lifetimes. The band structure of excitons is approximated by a parabolic dispersion with a given exciton mass and binding energy. In this paper we only model the lowest-lying exciton with mass $m_{11} = 0.21 m_e$ and energy $E_{11} = 1.24$ eV, where m_e is the bare electron mass [29,30]. Among the six phonon branches, we only consider the top four nonacoustic modes, since the former have negligible coupling with excitons [31]. Also, phonon bands are modeled as nearly flat bands in the vicinity of the scattering regions and their energy is taken from theoretical calculation for consistency [31]. We label each phonon mode using the standard group theory nomenclature, namely A, E_1, and E_2 phonons [32]. Table I lists the phonon modes considered in this work.

Each transition bears an inherent broadening arising from the many-body nature of the interaction. We assign a Lorentzian linewidth to each quasiparticle and use Matthiessen's rule to account for the total broadening of a scattering event. The values used in this work are shown

TABLE II. Exciton and phonon broadenings in meV.

E_{11}	A^i	E_1^i	E_2^i
45.7	1.8	2.9	2.9

in Table II and are taken from theoretical and experimental data [33–35].

Collision integrals and matrix elements. In the case of a four-leg scattering, the collision integral on the right-hand side of Eq. (1) can be written as

$$\left(\frac{\partial f_1}{\partial t}\right)_{12-34} = \frac{2\pi}{\hbar} \frac{1}{V_{BZ}^2} \sum_{\mathbf{G}} \int_{V_{BZ}^3} d\mathbf{k}_2 d\mathbf{k}_3 d\mathbf{k}_4 \left| g_{12}^{34} \right|^2 \delta_{\mathbf{k}} \, \delta_\epsilon \, P_{12}^{34}. \tag{A1}$$

The above equation describes the interaction between two particles in an initial state $|12\rangle$ that scatter into a final state $|34\rangle$. Each state is labeled by the wave vector quantum number, $\mathbf{k}_1$, $\mathbf{k}_2$, $\mathbf{k}_3$, and $\mathbf{k}_4$, respectively. Similarly, the individual populations of the initial and final states are f_1, f_2, f_3, and f_4. Equation (A1) is a fourth-order integral operator that represents the rate of change of population f_1 as a consequence of the interaction with f_2, f_3, and f_4. We have $g_{12}^{34} = \langle 12|\hat{V}|34\rangle = g(\mathbf{k}_1, \mathbf{k}_2, \mathbf{k}_3, \mathbf{k}_4)$; these are the matrix elements of the interaction $\hat{V}$ between the initial and the final state. In this work, g_{12}^{34} are approximated with averaged constant values obtained from the literature [36,37] or fitted to experiments when not available [25]. Energy and momentum conservation are enforced by

$$\delta_{\mathbf{k}} = \delta(\mathbf{k}_1 + \mathbf{k}_2 - \mathbf{k}_3 - \mathbf{k}_4 + \mathbf{G}),$$
$$\delta_\epsilon = \delta(\epsilon_1(\mathbf{k}_1) + \epsilon_2(\mathbf{k}_2) - \epsilon_3(\mathbf{k}_3) - \epsilon_4(\mathbf{k}_4)), \tag{A2}$$

where $\epsilon_i(\mathbf{k}_i)$ are the energy dispersion relations described above. And finally the population term P_{12}^{34} is given by

$$P_{12}^{34} = \bar{f}_1 \bar{f}_2 f_3 f_4 - f_1 f_2 \bar{f}_3 \bar{f}_4, \tag{A3}$$

where $\bar{f}_i = 1 \pm f_i$, and the plus and minus signs apply to bosonic and fermionic particles, respectively.

Light absorption. The absorption (or emission) of light is computed as the functional derivative of the collision integral with respect to the photon population [cf. Eq. (3)]. For example, given the above four-leg scattering, the quantity

$$\lambda_1(\mathbf{k}_1) = \frac{\delta}{\delta f_1} \left(\frac{\partial f_1}{\partial t}\right)_{12-34} \tag{A4}$$

is the probability rate of change of population f_1, as a consequence of the interaction with f_2, f_3, and f_4 [24].

[1] F. Wang, G. Dukovic, L. E. Brus, and T. F. Heinz, The optical resonances in carbon nanotubes arise from excitons, Science **308**, 838 (2005).

[2] J. A. Misewich, R. Martel, P. Avouris, J. C. Tsang, S. Heinze, and J. Tersoff, Electrically induced optical emission from a carbon nanotube FET, Science **300**, 783 (2003).

[3] M. Iwamura, N. Akizuki, Y. Miyauchi, S. Mouri, J. Shaver, Z. Gao, L. Cognet, B. Lounis, and K. Matsuda, Nonlinear photoluminescence spectroscopy of carbon nanotubes with localized exciton states, ACS Nano **8**, 11254 (2014).

[4] M. E. Portnoi, O. V. Kibis, and M. Rosenau da Costa, Terahertz applications of carbon nanotubes, Superlattices Microstruct. **43**, 399 (2008).

[5] M. Rosenau da Costa, O. V. Kibis, and M. E. Portnoi, Carbon nanotubes as a basis for terahertz emitters and detectors, Microelectron. J. **40**, 776 (2009).

[6] A. Högele, C. Galland, M. Winger, and A. Imamoğlu, Photon antibunching in the photoluminescence spectra of a single carbon nanotube, Phys. Rev. Lett. **100**, 217401 (2008).

[7] M. E. Sykes, M. Kim, X. Wu, G. P. Wiederrecht, L. Peng, Y. Wang, D. J. Gosztola, and X. Ma, Ultrafast exciton trapping at sp^3 quantum defects in carbon nanotubes, ACS Nano **13**, 13264 (2019).

[8] A. H. Brozena, M. Kim, L. R. Powell, and Y. Wang, Controlling the optical properties of carbon nanotubes with organic colour-centre quantum defects, Nat. Rev. Chem. **3**, 375 (2019).

[9] O. V. Kibis and M. E. Portnoi, Carbon nanotubes: A new type of emitter in the terahertz range, Tech. Phys. Lett. **31**, 671 (2005).

[10] L. Cognet, D. A. Tsyboulski, J.-D. R. Rocha, C. D. Doyle, J. M. Tour, and R. B. Weisman, Stepwise quenching of exciton fluorescence in carbon nanotubes by single-molecule reactions, Science **316**, 1465 (2007).

[11] F. Wang, G. Dukovic, E. Knoesel, L. E. Brus, and T. F. Heinz, Observation of rapid Auger recombination in optically excited semiconducting carbon nanotubes, Phys. Rev. B **70**, 241403(R) (2004).

[12] A. Jorio and R. Saito, Raman spectroscopy for carbon nanotube applications, J. Appl. Phys. **129**, 021102 (2021).

[13] L. Lüer, S. Hoseinkhani, D. Polli, J. Crochet, T. Hertel, and G. Lanzani, Size and mobility of excitons in (6, 5) carbon nanotubes, Nat. Phys. **5**, 54 (2009).

[14] Z. Zhu, J. Crochet, M. S. Arnold, M. C. Hersam, H. Ulbricht, D. Resasco, and T. Hertel, Pump-probe spectroscopy of exciton dynamics in (6, 5) carbon nanotubes, J. Phys. Chem. C **111**, 3831 (2007).

[15] C. A. Parra-Murillo, M. F. Santos, C. H. Monken, and A. Jorio, Stokes–anti-Stokes correlation in the inelastic scattering of light by matter and generalization of the Bose-Einstein population function, Phys. Rev. B **93**, 125141 (2016).

[16] S. Hughes and H. J. Carmichael, Phonon-mediated population inversion in a semiconductor quantum-dot cavity system, New J. Phys. **15**, 053039 (2013).

[17] R. Manson, K. Roy-Choudhury, and S. Hughes, Polaron master equation theory of pulse-driven phonon-assisted population inversion and single-photon emission from quantum-dot excitons, Phys. Rev. B **93**, 155423 (2016).

[18] J. H. Quilter, A. J. Brash, F. Liu, M. Glässl, A. M. Barth, V. M. Axt, A. J. Ramsay, M. S. Skolnick, and A. M. Fox, Phonon-assisted population inversion of a single InGaAs/GaAs quantum dot by pulsed laser excitation, Phys. Rev. Lett. **114**, 137401 (2015).

[19] C. Ferrante, A. Virga, L. Benfatto, M. Martinati, D. De Fazio, U. Sassi, C. Fasolato, A. K. Ott, P. Postorino, D. Yoon, G. Cerullo, F. Mauri, A. C. Ferrari, and T. Scopigno, Raman spectroscopy of graphene under ultrafast laser excitation, Nat. Commun. **9**, 308 (2018).

[20] A. Jorio, M. Kasperczyk, N. Clark, E. Neu, P. Maletinsky, A. Vijayaraghavan, and L. Novotny, Optical-phonon resonances with saddle-point excitons in twisted-bilayer graphene, Nano Lett. **14**, 5687 (2014).

[21] G. Gordeev, A. Jorio, P. Kusch, B. G. M. Vieira, B. Flavel, R. Krupke, E. B. Barros, and S. Reich, Resonant anti-Stokes Raman scattering in single-walled carbon nanotubes, Phys. Rev. B **96**, 245415 (2017).

[22] M. Steiner, H. Qian, A. Hartschuh, and A. J. Meixner, Controlling nonequilibrium phonon populations in single-walled carbon nanotubes, Nano Lett. **7**, 2239 (2007).

[23] I. Wadgaonkar, M. Wais, and M. Battiato, Numerical solver for the out-of-equilibrium time dependent Boltzmann collision operator: Application to 2D materials, Comput. Phys. Commun. **271**, 108207 (2022).

[24] M. Wais, K. Held, and M. Battiato, Numerical solver for the time-dependent far-from-equilibrium Boltzmann equation, Comput. Phys. Commun. **264**, 107877 (2021).

[25] S. Dal Forno, N. Komatsu, M. Wais, A. Mojibpour, I. Wadgaonkar, S. Ghosh, Y. Yomogida, K. Yanagi, K. Held, J. Kono, and M. Battiato, Origin of the background absorption in carbon nanotubes: Phonon-assisted excitonic continuum, Carbon **186**, 465 (2022).

[26] E. Hanamura and H. Haug, Condensation effects of excitons, Phys. Rep. **33**, 209 (1977).

[27] See Supplemental Material at http://link.aps.org/supplemental/10.1103/PhysRevB.110.125412 for the comparison between theory and experimental data, and for a detailed description of fermionic and bosonic statistics of the excitons.

[28] M. Zheng and B. A. Diner, Solution redox chemistry of carbon nanotubes, J. Am. Chem. Soc. **126**, 15490 (2004).

[29] D. C. Mattis and J. P. Gallinar, What is the mass of an exciton? Phys. Rev. Lett. **53**, 1391 (1984).

[30] M. S. Dresselhaus, G. Dresselhaus, R. Saito, and A. Jorio, Exciton photophysics of carbon nanotubes, Annu. Rev. Phys. Chem. **58**, 719 (2007).

[31] Y.-S. Lim, A. R. T. Nugraha, S.-J. Cho, M.-Y. Noh, E.-J. Yoon, H. Liu, J.-H. Kim, H. Telg, E. H. Hároz, G. D. Sanders, S.-H. Baik, H. Kataura, S. K. Doorn, C. J. Stanton, R. Saito, J. Kono, and T. Joo, Ultrafast generation of fundamental and multiple-order phonon excitations in highly enriched (6, 5) single-wall carbon nanotubes, Nano Lett. **14**, 1426 (2014).

[32] E. B. Barros, A. Jorio, G. G. Samsonidze, R. B. Capaz, A. G. S. Filho, J. M. Filho, G. Dresselhaus, and M. S. Dresselhaus, Review on the symmetry-related properties of carbon nanotubes, Phys. Rep. **431**, 261 (2006).

[33] F. Katsutani, W. Gao, X. Li, Y. Ichinose, Y. Yomogida, K. Yanagi, and J. Kono, Direct observation of cross-polarized excitons in aligned single-chirality single-wall carbon nanotubes, Phys. Rev. B **99**, 035426 (2019).

[34] K. Kaasbjerg, K. S. Thygesen, and K. W. Jacobsen, Unraveling the acoustic electron-phonon interaction in graphene, Phys. Rev. B **85**, 165440 (2012).

[35] C.-H. Park, F. Giustino, M. L. Cohen, and S. G. Louie, Electron-phonon interactions in graphene, bilayer graphene, and graphite, Nano Lett. **8**, 4229 (2008).

[36] E. Malic and A. Knorr, *Graphene and Carbon Nanotubes: Ultrafast Relaxation Dynamics and Optics* (Wiley, 2013).

[37] A. Jorio, G. Dresselhaus, and M. S. Dresselhaus, *Carbon Nanotubes: Advanced Topics in the Synthesis, Structure, Properties and Applications*, Topics in Applied Physics (Springer, 2008).